Use of Plasmon Coupling to Reveal the Dynamics of DNA Bending and Cleavage by Single EcoRV Restriction Enzymes

Björn M. Reinhard[*,†,‡], Sassan Sheikholeslami[†,§], Alexander Mastroianni[†,§], A. Paul Alivisatos[†,§] & Jan Liphardt[*,‡,¶]

[*]Physics Department and [†]Chemistry Department, University of California at Berkeley, [‡]Physical Biosciences Division and [§]Materials Sciences Division, Lawrence Berkeley National Laboratory, Berkeley, California 94720, USA

[¶]Email: Liphardt@physics.berkeley.edu

Classification: Biological Sciences / Biophysics

Words in the Abstract: 170

Total Characters: 45062

Number of text pages: 13

Pairs of Au nanoparticles have recently been proposed as "plasmon rulers" based on the dependence of their light scattering on the interparticle distance. Preliminary work has suggested that plasmon rulers can be used to measure and monitor dynamic distance changes over the 1 to 100nm length scale in biology. Here, we substantiate that plasmon rulers can be used to measure dynamical biophysical processes by applying the ruler to a system that has been investigated extensively using ensemble kinetic measurements: the cleavage of DNA by the restriction enzyme EcoRV. Temporal resolutions of up to 240 Hz were obtained, and the end-to-end extension of up to 1,000 individual dsDNA enzyme substrates could be simultaneously monitored for hours. The kinetic parameters extracted from our single molecule cleavage trajectories agree well with values obtained in bulk through other methods, and confirm well-known features of the cleavage process, such as DNA bending prior to cleavage. New dynamical information is revealed as well, for instance, the degree of softening of the DNA just prior to cleavage. The unlimited lifetime, high temporal resolution, and high signal/noise make the plasmon ruler a unique tool for studying macromolecular assemblies and conformational changes at the single molecule level.

Introduction

The optical characterization of the function and dynamics of single biological molecules and complexes such as molecular motors (1-3), RNA ribozymes (4) and DNA helicases and binding proteins (5, 6) is an important tool for biomedical research (for review see (7-9)). Single molecule techniques are powerful tools to study the dynamics of biological systems, since they are free from ensemble averaging (9). The predominant technique for optical single molecule dynamic studies is Fluorescence Resonance Energy Transfer (FRET) between individual organic donor and acceptor dye molecules (10, 11). FRET has proven to be an extremely effective tool for revealing the dynamics of molecular machines and monitoring their composition. However, conventional organic dyes typically photobleach after absorbing about 10^7 photons and exhibit complex photophysics including long-lived dark-states (12). Single molecule FRET studies thus remain challenging due to low signal/noise, limited continuous observation time, limited accessible distance range, and probe blinking.

We recently reported an alternative method for dynamic distance measurements on the nanometer scale using pairs of individual 40 nm gold particles (13). When two gold particles approach within two particle diameters, the collective oscillations of the conductions electrons in the particles (their *plasmons*) couple (14-21) in a distance dependent matter. With decreasing interparticle distance, the plasmon resonance wavelength red-shifts (22) and the scattering cross-section increases (23). Individual pairs of biopolymer linked noble metal nanoparticles therefore act as "plasmon rulers". By variation of the nanoparticle's shape and structure (hollow/solid), the plasmon wavelength

can be fine-tuned over a wide spectral range from the blue into the infrared (24, 25). The resulting benefits of plasmon coupling for sensitive analytical bulk application has been pioneered by Mirkin and coworkers in their colorimetric detection scheme (16)

Plasmon rulers have a nearly unlimited lifetime, can be used to monitor comparatively large distance changes, and are very bright. If the scattering background can be eliminated, a single 40 nm gold particle has the light emitting power of several thousand organic dyes (26). The inherent brightness of these probes makes them good candidates for highly parallel single molecule assays able to reveal the dynamics of biological processes and biopolymers. A drawback of plasmon rulers compared to FRET methods is the relatively large size of the nanoparticles compared to organic fluorophores (~ 30-40 nm versus ~ 1 nm).

Our focus is the measurement of DNA bending and deformation by single enzymes, an experimental geometry in which the benefits of unlimited lifetime and lack of bleaching outweigh the disadvantage of larger probe size. DNA bending plays a crucial role in determining the specificity in DNA-protein recognition (27), in transcription regulation (28-32), and in DNA packaging (33, 34). Typically, these DNA bending processes are quite slow (ms timescales) and it is highly desirable to be able to monitor a particular piece of DNA for extended durations (milliseconds to days), so that the effects of enzyme concentration, ionic strength changes, pH changes, etc. can be accurately followed.

Here we use plasmon rulers to investigate the dynamics of the EcoRV catalyzed DNA cleavage reaction in a highly parallel, high bandwidth (up to 240 Hz) single molecule assay. We picked the EcoRV restriction enzyme since it is a member of the type II restriction endonucleases, which are important paradigms for the study of protein-nucleic acid interactions (35-38). They catalyze phosphodiester bond cleavage with very large rate enhancements and superb sequence (EcoRV recognition sequence: 3'-CTA↓TAG-5') selectivities. The EcoRV endonuclease transiently bends its DNA substrate and the bend angle is well known from crystal structures to be approximately 50° (39, 40).

Using plasmon rulers, we were able to follow certain steps in the catalytic cycle of EcoRV and directly observe DNA bending immediately preceding cleavage,

confirming the standard model of how this enzyme works. By analysis of the interparticle potentials, we were also able to see the softening of the DNA resulting from its interactions with the enzyme prior to cleavage.

Results and Discussion

Three technical challenges needed to be overcome to be able to use plasmon rulers to monitor the dynamics of single enzyme-DNA complexes. First, nonspecific protein-particle interactions needed to be suppressed. Second, methods were needed to synthesize homogeneous samples of plasmon rulers. Third, the plasmon rulers' temporal resolution needed to be improved from ~ 1 Hz (13) to 240 Hz.

To eliminate non-specific interactions between the gold surface and the enzyme, we used a stepwise ligand exchange strategy in which we passivated the particle surfaces with biocompatible (41) low molecular mass polyethylene glycols (PEGs). We then synthesized DNA linked nanoparticle dimers (plasmon rulers) with double stranded DNA spacers between 30-60bp using a liquid phase DNA-programmed assembly strategy followed by gel-electrophoretic purification (**Fig. S1**). As confirmed by TEM, this approach produces enriched samples of dimers. Since interparticle distances in aqueous solution cannot be inferred from TEM measurements, we measured the pair distribution functions of isolated plasmon rulers using small angle x-ray scattering (**Fig. S1**). The distributions contain strong dimer peaks of separated 40 nm gold particles and confirm that our synthetic strategy leads to DNA tethered dimers (**Fig. S1**).

To increase the temporal resolution of the plasmon ruler measurements, we investigated the dependence of the scattering intensity on the interparticle distance. In previous applications of plasmon rulers, we utilized the distance dependence of the resonance wavelength to measure distances and distance changes in DNA (13, 22). However, the spectral analysis of individual plasmon rulers relies on the dispersion of light, forcing us to integrate photon counts for several hundred milliseconds to obtain a detectable signal in our set-up. This is too slow to resolve the dynamics of biological processes such as enzymatic DNA bending and cleavage, which typically occur on timescales of micro to milliseconds.

We reasoned that intensities can be collected with a much higher temporal resolution than spectral information, since no dispersion is required. It can be shown that – like the plasmon resonance wavelength – the scattering cross-section of a coupled pair of dimers depends on the interparticle distance. In a first approximation, each particle is treated as a simple dipole. Using this assumption, the cross-section of two coupled

particles with identical diameters is proportional to the square of the pair polarizability Λ, for which the following expression can be derived by averaging over longitudinal and perpendicular plasmon modes (23):

$$\Lambda = \frac{\eta}{3}\left[\frac{1}{1-2\eta\left(R/R_P\right)^3} + \frac{2}{1+\eta\left(R/R_P\right)^3}\right], \quad with\ \eta = \frac{\varepsilon - \varepsilon_m}{\varepsilon + 2\varepsilon_m} \qquad \textbf{Eq. 1}$$

where ε is the wavelength dependent dielectric function of gold (42), ε_m is the dielectric constant of the surrounding medium, R the interparticle distance, and R_P is the particle radius. We set the dielectric constant of the medium to ε_m = 1.6, as before (22). **Eq. 1** is a highly simplified description of the relationship between scattering cross-section and interparticle distance; among other things, we are using a dielectric function for an idealized bulk metal in an isotropic environment and we are neglecting multipole contributions. Therefore, we expect qualitative rather than quantitative agreement of **Eq. 1** with experiment.

To validate this approach, we recorded the scattering spectra of EcoRV catalyzed DNA cleavage reactions using an intensified CCD detector. The biological aspects of this experiment are described subsequently; for our purposes here it is only important to know that DNA cleavage by the EcoRV enzyme leads to plasmon ruler disassociation. As the DNA tethering the particles is cut, the interparticle distance suddenly increases, and consequently the scattering wavelength blue-shifts (**Fig. 1**) in a well-understood manner (22). The particle plasmons cease to couple when the dimers dissociate and consequently their resonance wavelengths and scattering cross-sections relax to the monomer values.

To correlate the spectral shifts with changes in scattering intensity, we computed the total scattering intensities by integrating photon counts on the spectrometer over all wavelengths for six individual wavelength trajectories. The average Pearson correlation coefficient between integrated intensity and peak wavelength in individual trajectories is r = 0.92, confirming that color (peak wavelength) and scattering intensity are correlated and that the scattering intensity can be used to monitor interparticle distance. Ultimately, we achieved temporal resolutions of 240 Hz in a 20 μm x 20 μm field of view. To

increase the throughput, we eventually collected data with a lower temporal resolution (85 Hz) but in a larger field of view of approximately 40 μm x 40 μm.

Highly Parallel Single EcoRV Restriction Digestion Assay

Having in hand enriched samples of surface passivated plasmon rulers and a method for monitoring the ruler's interparticle separation with high temporal resolution, we set out to monitor the bending and cleavage dynamics of single EcoRV enzymes. In a first set of experiments, we monitored the catalytic turnover of the enzyme by following many plasmon rulers in parallel under various conditions using a color camera. We immobilized plasmon rulers on the surface of a glass flowchamber via a Biotin-Neutravidin bond between the Biotin functionalized particle and the surface (**Fig. 2a**). After equilibrating the chamber with 10 mM Mg^{2+} reaction buffer, we introduced the EcoRV restriction endonuclease and monitored the plasmon rulers' color and intensity. Due to the brightness of the plasmon rulers (scattering cross-section of 40 nm particles, C_{sca} = 130 nm^2) (26) it was possible to simultaneously monitor 500 - 1500 plasmon rulers using a low numerical aperture and low magnification 40x objective. The complete field of view in these experiments is limited to 150 μm x 100 μm by our camera and chosen magnification.

Upon addition of the enzyme, some plasmon rulers exhibited sudden intensity drops (**Fig. 2b**, **Movie S1**). The green dots are individual dimers and the red arrows denote locations of these intensity drops. Complete detachment of the dimer from the surface cannot account for the observed intensity drops, since a dim green spot – corresponding to a single surface-immobilized gold particle – remains after the intensity drop. Rather, the ruler dissociation events are due to enzymatic DNA cleavage, as we now establish. First, plasmon rulers constructed from DNA lacking the EcoRV restriction site do not dissociate (**Fig. 3a)**: only 11 intensity drops are seen with the control DNA, whereas for dimers with the EcoRV recognition site, hundreds of dimer dissociations were observed. Second, the addition of Ca^{2+} to the reaction buffer dramatically reduces the number of intensity drops **(Fig. 3b)**. Ca^{2+} is a well characterized inhibitor of DNA cleavage by EcoRV (43). In our experiments, the first order rate constants of the intensity drops decreased from 0.036 s^{-1} (no Ca^{2+}) to 0.004 s^{-1} (2 mM Ca^{2+}). Taken together, the

observed sequence specificity and the inhibition of cleavage reaction by Ca^{2+} confirm that the observed dimer dissociation is the result of DNA cleavage by the EcoRV restriction endonuclease.

Plasmon rulers with 30bp spacers exhibit a lower cutting rate than the dimers with longer spacers (**Fig. 3a**), probably due to steric hindrance. According to the wormlike chain model for DNA (44) (contour length L = number of bases / 10.5 * 3.4 nm, persistence length P = 53 nm) (45), the interparticle distance for 30bp DNA spacers is 9.42 nm compared to 12.69 and 18.31 nm for 40 and 60bp respectively. The PEG brush (L=4.1 nm, P=2 nm) adds about 6 nm to the effective particle diameter. This leaves a gap of about 3.4 nm for the enzyme in case of the 30bp spacer compared to 6.4 nm in case of the 40bp spacer. It is known that the binding of one molecule of EcoRV covers about 15bp = 4.79 nm of DNA (39). Presumably, the binding step (**Fig. 2a**, step I) is sterically hindered by the PEG brush in the case of the 30bp spacers, slightly reducing cleavage kinetics.

Dynamics of Single EcoRV Catalyzed DNA Cleavage Reactions

After identifying the sudden intensity drops as dimer disassociation resulting from DNA cleavage by EcoRV, we analyzed the intensity vs. time traces of individual cutting events at high temporal resolution. According to the standard model of DNA cleavage by EcoRV (**Fig. 2a**), DNA cutting occurs in a bent state (bend angle ~ 50°). Based on an end-to-end distance from the WLC model and a 50° bend, the interparticle distance should decrease by 0.95 nm (Δ_{30bp}), 1.20 nm (Δ_{40bp}), 1.85 nm (Δ_{60bp}) due to DNA bending by EcoRV. Judging from the inverse pair polarizability – distance dependence given in **Eq. 1**, bending should slightly increase the scattering intensity. Given that the predicted distance changes amount to only ~ 10% of the DNA spacer length, this is a challenging test case for the sensitivity of the plasmon rulers.

Our search for intensity changes due to bending was greatly facilitated by the large intensity drop upon dimer dissociation, since it allowed us to locate the disassociation time with high precision and thus also constrain the region that needed to be analyzed for evidence of DNA bending. Using the dissociation event as a fiduciary time-point, we calculated the average intensity preceding the dissociation from all

recorded trajectories. Although temporal resolutions of 240 Hz could be achieved (see e.g. **Fig. 4a**) we typically monitored the plasmon rulers' intensity at 85 Hz to increase the throughput with the larger field of view.

The average intensities as a function of time are shown in **Figs. 4b-d**. For both the 30 and 40bp DNA spacers, there is a significant increase in average scattering intensity of up to 1.5% immediately before dimer dissociation. Consistent with the known inverse relationship between sensitivity and spacer length (22), the average intensity for the 60bp spacer remains nearly constant. The measured average intensity changes (1.5% ± 0.8 (30bp), 1.6% ± 0.9 (40bp) and -0.5% ± 0.8 (60bp)) are consistently smaller (about 2-fold) than the estimates obtained from the order-or-magnitude calculation (**Eq. 1**, 2.6% (30bp), 2.0% (40bp) and 1.4% (60bp)). Given the large number of assumptions that went into those estimates, including the magnitude of the bend caused by the EcoRV enzyme, the end-to-end extension of the DNA, the thickness of the PEG brush, the uncertainty in the dielectric function, and the omission of multipole terms, the agreement between theory and experiment is considerably better than expected.

Is DNA bending by the EcoRV restriction enzyme the most probable explanation for the observed intensity increases before the cut? The scattering intensity depends – next to the interparticle distance – also on the dielectric constant of the surrounding medium. It is therefore conceivable that enzyme binding (**Fig. 2a**, step II) and not DNA bending (**Fig. 2a**, step III) causes the observed intensity change by a local change of the refractive index. Therefore, we decoupled binding from bending by letting EcoRV react with 40bp plasmon rulers in the absence of divalent metal ions (K_D in the absence of Mg^{2+}: ~ $1x10^{-8}$ M) (46), preventing cleavage but not binding (47). We then flushed the unbound enzyme out of the chamber with divalent-free buffer. Finally, we introduced Mg^{2+}, allowing the bound enzymes to cleave their DNA substrate. As shown in **Figs. S2&S3**, these trajectories exhibit intensity jumps preceding dimer dissociation, confirming our interpretation of the intensity jumps as DNA bending and not protein-DNA binding or sticking of proteins to the gold particles. Thus, the high intensity state most likely corresponds to steps III – IV in **Fig. 2a** in which the DNA is bent by 50°.

Individual traces show large variations in bending times. The trajectory shown in **Fig. 4e** exhibits a spike in intensity before the dimers dissociate. In this trajectory only

the very last frame before dissociation has an increased intensity whereas in **f** and **g** the dwell times are on the order of a few seconds (**f**) and a few tens of seconds (**g**) respectively. Student's t tests show that in ~ 76 % of all 40bp dimer trajectories with "high intensity states" exceeding 100 frames, high and low intensity states differ significantly ($p < 0.05$). In 4% of all collected trajectories, the large drop in intensity due to the DNA cleavage is preceded by a smaller intensity drop as shown in **Fig. 4h**. This behavior suggests two subsequent DNA cutting events in dimers that have two instead of one DNA tether. The cleavage of the first tether does not lead to the dissociation of the particles but only to a slight increase in equilibrium distance. The low probability of this behavior suggests that most of the dimers are indeed tethered by only one DNA molecule.

Having assigned the intensity jumps to DNA bending by the EcoRV enzyme and having determined the average intensity changes prior to DNA cleavage/particle pair disassociation, we built-up distributions of the duration of the high intensity state for the 30 and 40bp dimer trajectories. The results of the dwell time analyses are shown in **Fig. 5a**. The cumulative dissociation probability is plotted in **Fig. 5b**. In these plots the percentage of dimers that have been cleaved is plotted against the time they spend in the high intensity state. Exponential fits to the decay curves in **Fig. 5b** give rate constants of $k_{30} = 0.50\ s^{-1}$ (30bp, R^2=0.94) and $k_{40} = 0.46\ s^{-1}$ (40bp, R^2=0.91). The similarity of the two rate constants is in agreement with the assertion that the trajectories comprise molecular events like DNA bending, DNA hydrolysis and product release but not DNA binding, which is expected to be much slower in case of the 30bp spacer due to steric hindrance.

The catalytic cycle of the EcoRV endonuclease with short (7-14bp) DNAs as substrate has been investigated in bulk using FRET, stopped flow fluorescence, fluorescence anisotropy and quench-flow methods (46, 48, 49). These studies found that the turnover rate k_{cat} is limited by the rates of the DNA hydrolysis and product release (**Fig. 2a**, steps IV & V), which are approximately equivalent in magnitude (46), whereas DNA bending is nearly simultaneous with binding. It is therefore possible to compare k_{30} and k_{40} with k_{cat}. The determined k_{30} and k_{40} are lower than the bulk steady state $k_{cat} = 0.7\ s^{-1}$ for 10 mM Mg^{2+} and are closer to the bulk k_{cat} for 4 mM Mg^{2+} (49). Interestingly, our

rate constants are very close to the first order rate constant of 0.4 s^{-1} as obtained by FRET for the later stages of the reaction cycle (46). Thus, although deviations from the bulk rates are to be expected in our experiments (in our case, the DNA substrate is tethered on the surface and has less configurational freedom, the gold probes may slow the dynamics of the enzymatic reaction, and there may be a small non-zero force between the two particles (50)), such deviations are therefore small (not more than 0.2 s^{-1}).

In addition to elucidating the dynamics of DNA bending and cleavage by EcoRV, the scattering trajectories can also be used to estimate the interaction potential ϕ between the two DNA-linked nanoparticles. Just as the probability P of a DNA-tethered microsphere to be at a certain height h above a surface depends on the potential between the surface and the microsphere (51, 52), the probability of an individual plasmon to be in a certain intensity state I is related to the interparticle potential ϕ. The interparticle potential ϕ determines the equilibrium interparticle distance. We used the relationship $P(I) \sim exp(-\phi(I)/kT)$ to construct the potential ϕ in the bent and unbent states for the 40bp plasmon rulers. $P(I)$ is obtained from scattering intensity histograms of the high and low intensity states from single scattering trajectories with more than 100 frames in the high intensity state (**Fig. 5c**). The resulting average potentials for the bent and unbent states are shown in **Fig. 5d**. The repulsive part of the interparticle potential is mainly determined by the surface coating of the particles and therefore identical for the bent and unbent states. Consequently, the arbitrary additive constant of the potentials has been chosen so that the repulsive parts of the potentials coincide. Comparison of the two potentials reveals that the bent state is energetically disfavored by $\Delta\phi = 1.2\ kT$.

This interpretation of the intensity distributions (**Fig. 5c**) must take various error sources into account. Specifically, the measured intensity distributions are convolutions of longitudinal and transverse fluctuations of the top particle with respect to the surface-bound particle and experimental noise. We are interested only in the variations of the interparticle separation, corresponding to the end-to-end distance of the tethering DNA. Assuming that the transverse fluctuations and the experimental noise are free from systematic errors, then their combined effect will be to broaden the intensity distributions. In consequence, the intensity distributions and all derived quantities represent upper bounds on the magnitude of the longitudinal fluctuations, and the potentials shown in

Fig. 5d are lower bounds constraining the shape of the unknown and not directly measurable true potentials. Our $\Delta\phi$ of 1.2 kT is therefore a lower bound on the true energy difference between the bent and straight state. Indeed, the WLC predicts an energy difference of 1.6 kT for a 50° kink in a 40bp DNA molecule (53) exceeding our experimental value by 25%.

A second quantity, the relative change of the width of the two potentials, is less subject to various experimental errors since they should equally affect both intensity distributions and since the assumption of coincidence of the repulsive parts of the potentials is not needed. Parabolic fits $\phi = 1 + bI^2$ to the superimposed potentials in **Fig. 5e** reveal that b_{bent} is ~ 27.3% smaller than b_{unbent} (b_{bent} = 0.016, b_{unbent} = 0.022). The wider potential for the bent DNA state indicates that the interaction of the DNA with the enzyme decreases the spring constant of the DNA. This effect could account for the difference between the experimental and the predicted $\Delta\phi$ and has mechanistic implications. By reducing the DNA stiffness, the enzyme decreases the energetic bias of the bent state and reduces the activation energies of the rate determining steps – phosphate backbone hydrolysis and DNA dissociation – both of which occur in the bent state (**Fig. 2a**).

The plasmon ruler is a new method for measuring dynamical distance changes in single molecule biophysics experiments. In this work, we have taken an important step forward in validating the use of this type of ruler, by performing an in depth study of DNA cleavage by the EcoRV restriction enzyme, a process that has previously been investigated by numerous established techniques. The plasmon ruler experiments recapitulate what is known from prior ensemble kinetic studies and single molecule FRET experiments, indicating that the Au particles do not significantly perturb the system. In addition, the plasmon ruler experiments afford the possibility of studying fluctuations in the bending of the DNA, which can be used to determine the potential energy change between the straight and bent states of the DNA. The plasmon ruler is now sufficiently well developed to be used as a tool to study a wide range of biological processes. The ability of the ruler to operate over extended time scales and to be effective in measuring distances over the 1 to 100 nm range make it a unique tool for studying macromolecular assemblies and conformational changes at the single molecule level.

Methods

General. Aqueous solutions of 40nm gold particles with a concentration of 9.0×10^{10} particles/mL were purchased from Ted Pella. Freshly deionized water from a Millipore water system was used for all experiments. All buffers were filtered with a 0.2 μm Millipore filter directly prior to use. Trithiolated oligonucleotides were purchased from Fidelity Inc.

Passivation and Bulk Assembly of Plasmon Rulers. We applied a scheme of sequential ligand exchanges to functionalize and passivate 40 nm gold particles. In the first step, the citrate protected 40nm gold particles (concentration ~ 9.0×10^{10} particles/ml) purchased from Ted Pella were reacted with bis(p-sulfonatophenyl)phenylphosphine (BSPP) dipotassium salt, at the concentration of 1mg per 1ml of colloids. The particles were stirred with the BSPP for at least 8 hours before cleaning. The particles were washed twice by centrifugation (5000 rpm, 15 min) and resuspension in T40 (40mM NaCl, 10mM Tris, pH8). After resuspension the gold particle concentration is approximately 1.8×10^{12} particles/ml. The particles are split into two separate batches for the functionalization with complementary single stranded oligonucleotides (ssDNA). We used ssDNAs of 30, 40 and 60 nucleotides. The trithiolated ssDNA is first pre-incubated with a 1,000-fold excess of BSPP for 1 hour to reduce the disulfide bond of the protected ssDNAs before adding to the nanoparticle solutions at a ratio of 25 ssDNAs per particle. Then the mixture is left to react for 8 hours. The trithiolated ssDNA was chosen to enhance the anchor strength of the biopolymer (bond energy of a single Au-S bond: ~ 40 kcal/mol (54, 55)) and to decrease the flexibility of the DNA-thiol linker through multiple anchor points. The addition of salt was a prerequisite for successful functionalization of the particles with the ssDNAs.

Next, two different surface chemistries are added to the particle batches with complementary ssDNA (**Fig. S1a**). In the first batch, the ssDNA-particle solutions are reacted with a low molecular weight (458.6 g/mol) thiolated carboxy terminated polyethylene glycol (PEG) at a ratio of 1:100,000. In the second batch, the thiolated carboxy terminated PEGs are mixed with a thiolated biotin terminated PEG in a 25:1

ratio and reacted at the same total PEG concentration. The ssDNA-particle mixtures are incubated with the PEG ligands for at least 8 hours prior to cleaning. The PEG protected ssDNA functionalized particles are cleaned of excess reagent by centrifugation (5000 rpm, 15 min) and resuspension in T40. After two washing steps the particles are resuspended in 160mM NaCl 10mM Tris pH8 prior to annealing. Equivolume aliquots of the two different batches with complementary ssDNA were added together and left for 8 hours at room temperature to anneal the ssDNA.

The nanoparticle dimers were purified from monomers and higher order aggregates by gel electrophoresis (**Fig. S1b**) (56). The annealed particle mixtures were mixed with 1/5 volume Ficoll 400 loading buffer solution and loaded into 1% agarose gels. The gels were run horizontally at a fixed potential of 175 volts for 15 minutes with 0.5x Tris-Borate buffer as running buffer. After running the gels, the particle mixtures were found to be in discrete bands, with the second band from the top corresponding to the nanoparticle dimers. These bands were manually extracted from the gels and collected into an electroelution chamber. The dimers were then isolated from the gel via eletroelution. The isolated dimers were characterized by transmission electron microscopy, TEM (**Figs. S1c-d**), and small angle x-ray scattering, SAXS (**Fig. S1e**).

Optical Setup. Single molecule measurements were performed in a Zeiss axioplan2 upright microscope with a darkfield condenser. The darkfield microscope as described in previous publications (13, 22) was modified by the addition of an Andor iXon EM^{+} CCD detector (512x512 pixel chip) on the imaging port of the Acton SpectraPro 2300i spectrometer.

Surface Immobilization of Plasmon Rulers. The flow chambers were prepared by, first, incubating for 15 minutes with a solution of 1 mg/ml BSA-biotin [Roche] and then flushed with 300 µl T50 (50mM NaCl, 10mM Tris pH8). Next, the chambers were reacted with a solution of 1 mg/ml Neutravidin [Pierce, 31000] for 15 min and flushed with 300 µl T50. Subsequently, the chambers were incubated with SuperBlock [Pierce, 37515] for 45 minutes and flushed again with 300 µl T50.

Next, a dilute solution of plasmon rulers was flushed into the chamber. The plasmon rulers bind only with the biotinylated particle to the Neutravidin coated glass surface, while the non-biotinylated particle is free to move in solution. Control experiments verified that non-biotinylated, pegylated particles do not stick to the passivated glass surfaces. In the last step the chamber was equilibrated with EcoRV reaction buffer (100 mM Tris-HCl, 100 mM NaCl, 10 mM $MgCl_2$, 1 mM Dithiotreitol (DTT), pH 7.9).

Single Molecule Experiments. After equilibration of the chambers with reaction buffer, 40 units of EcoRV restriction endonuclease [New England Biolabs] in 200 μL reaction buffer was flushed into the chamber (EcoRV concentration ~1.75 nM). The scattering intensities of the plasmon rulers in the field of view were continuously monitored with a color camera (Roper Scientific, Coolsnap cf) or for faster temporal resolution with the Andor CCD detector. To correlate intensity and wavelength information, we recorded the scattering spectra of individual plasmon rulers during the EcoRV catalyzed cleavage reaction.

To prebind EcoRV enzyme to plasmon rulers, we incubated the plasmon rulers with EcoRV (4.4 nM) for approximately 1 min in Mg^{2+} free buffer (50 mM Tris-Hcl, 100 mM NaCl). Then we flushed the chamber with buffer (50 mM Tris-Hcl, 100 mM NaCl) to remove excess enzyme. Subsequently, reaction buffer containing Mg^{2+} was introduced and we started recording.

Data Analysis. By inspection of the movies recorded with the Andor CCD detector using software provided by the manufacturer, we detected all those dimers in the field of view that showed a sudden intensity drop. The movies were then imported into Matlab, where the exposed pixels were manually marked with a box. The CCD detector has a pixel size of 16μm x 16μm, and most of the light scattered from individual plasmon rulers is collected in one pixel. The intensity trajectories of individual plasmon rulers were calculated as sequence of the most intense pixels in the defined boxes. All of the recorded trajectories contained a clear drop in intensity that was set to 0 ms.

For the analysis of the average scattering intensity before dimer dissociation (recorded at 85 Hz), we superimposed all trajectories for a given spacer length. First, we calculated the average scattering intensities over defined intervals preceding dimer dissociation for each trajectory (interval lengths: 1770.0 ms, 1180.0 ms, 885.0 ms, 559.0 ms, 472.0 ms, 354.0 ms, 236.0 ms, 118.0 ms, 59.0 ms, 23.6 ms). Within each trajectory the average intensity of the longest time interval was set to 1. Then the normalized intensities for each time interval were averaged over all trajectories.

We thank Merek Siu, Stephanie Hsiao and Harish Agarwal. This work was supported in part by the University of California, Berkeley (JTL), the Hellman Faculty Fund (JTL), the Sloan foundation (JTL), the Searle foundation (JTL), and the US Department of Energy, Energy Biosciences Program (JTL) and the Director of Basic Energy Biosciences, Materials Science and Engineering Division (APA)(Contract # DE-AC02-05CH11231).

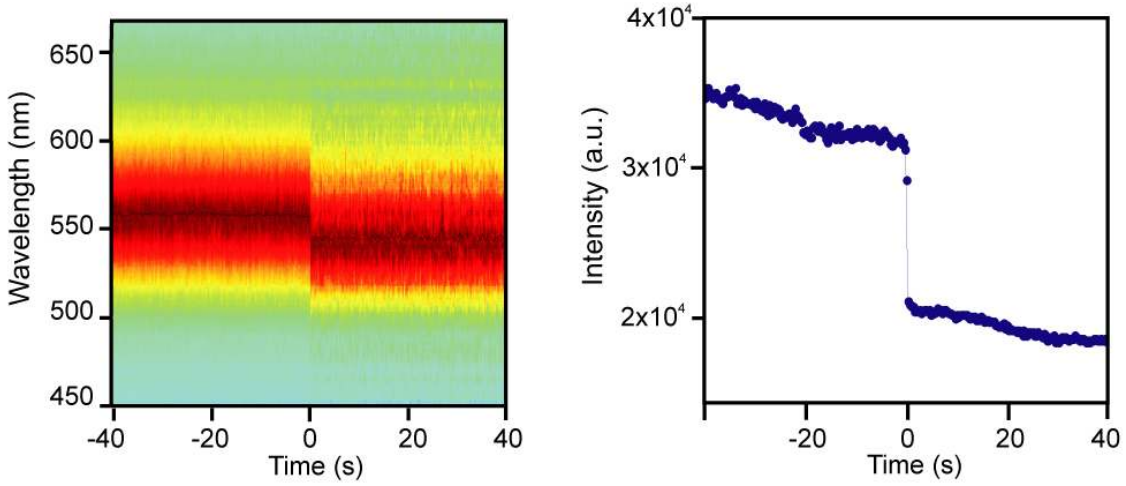

Fig. 1. Correlation of plasmon resonance wavelength and scattering intensity. Scattering wavelength (left) and integrated intensity (right) during EcoRV catalyzed DNA tether cleavage reaction recorded at 2Hz. Dimer dissociation leads to a sudden spectral blueshift (left) and a drop in total intensity (right). Spectral shift and change in total intensity are highly correlated (Pearson correlation coefficient > 0.9).

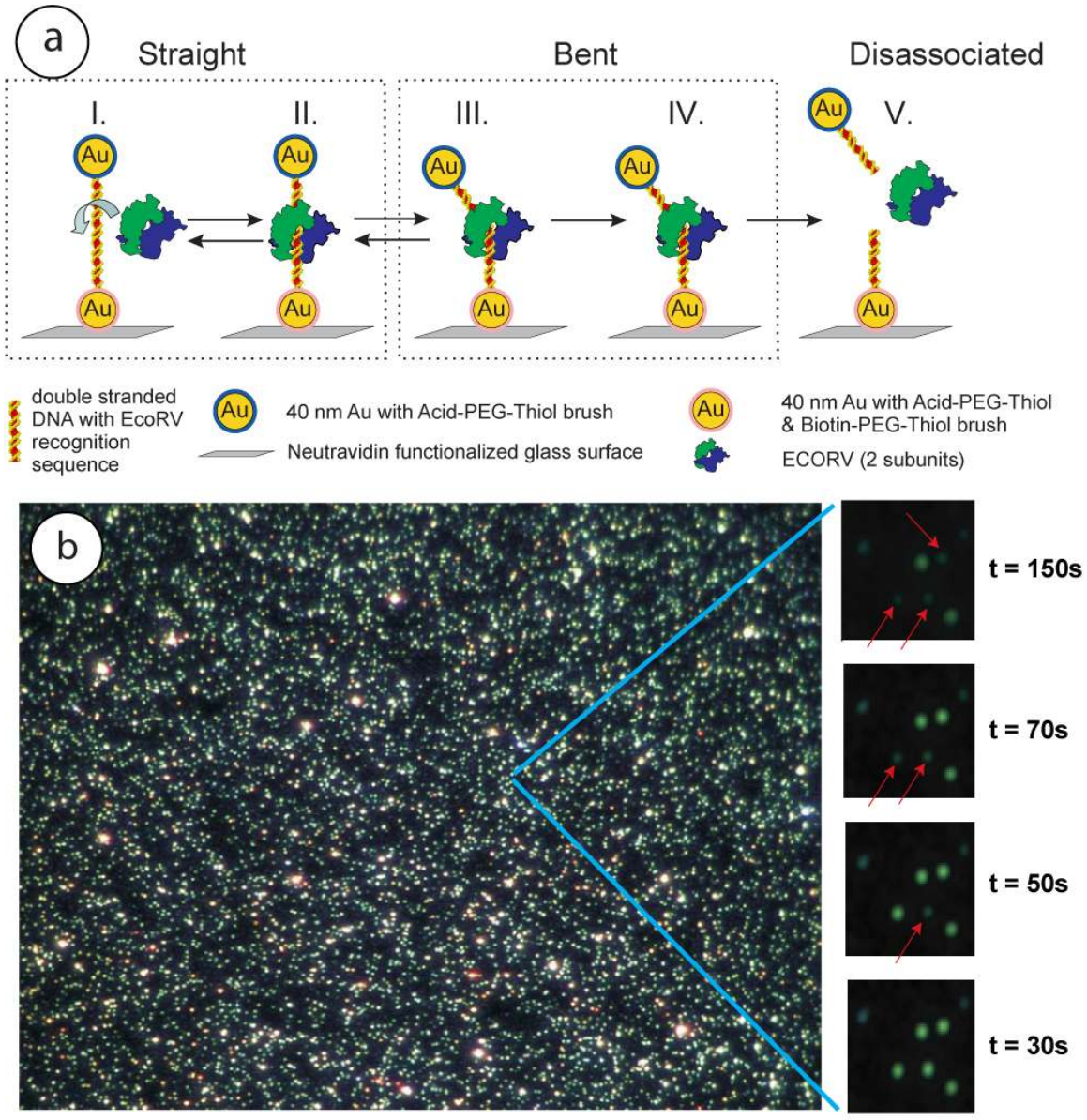

Fig. 2. Highly parallel single EcoRV restriction enzyme digestion assay. (*a*) The plasmon rulers are immobilized with one particle to a glass surface via Biotin-Neutravidin chemistry. The homodimeric EcoRV enzyme binds nonspecifically to DNA bound between the particles (I), translocates and binds to the target site (II), bends the DNA at the target site by ~50° (III), cuts the DNA in a blunt-ended fashion by phosphoryl transfer (57) (IV) and subsequently releases the products (V). (*b*) 150 µm x 100 µm field of view with surface immobilized plasmon rulers. Individual dimers are visible as bright green dots. Dimer dissociation upon EcoRV catalyzed DNA cleavage leads to a strong change in scattering intensities. The dimers are converted into monomers as shown for selected particles (red arrows, right side bar). EcoRV is added at t = 0s. A movie of the restriction digestion in the complete field of view is provided in the Supporting Information (Movie S1).

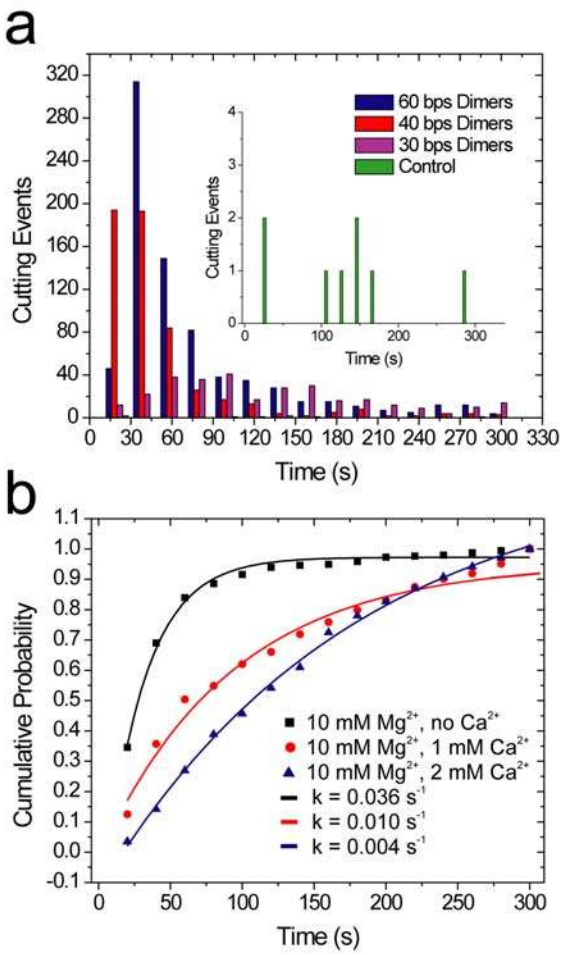

Fig. 3. Statistical analysis of EcoRV restriction digestion of plasmon rulers. (*a*) The cleavage reaction is highly specific. For all DNA spacers with an EcoRV restriction site, hundreds of cutting events are observed, in the control experiments (60 bps dimer) without a restriction site, the cutting efficiency is almost zero. Each histogram contains the combined results of two independent cutting experiments per spacer length performed with similar surface coverage. (*b*) Percentage of plasmon rulers that have been cleaved as function of time for increasing Ca^{2+} concentrations. First order kinetic fits are included as continuous lines. EcoRV requires Mg^{2+} as a natural cofactor to catalyze DNA cleavage. Ca^{2+} can replace Mg^{2+} and facilitates formation of the enzyme-DNA complex but the resulting complex does not catalyze the phosphodiester bond cleavage. Ca^{2+} inhibits the cleavage reaction in the presence of Mg^{2+}. A Mg^{2+} concentration of 10 mM was retained throughout.

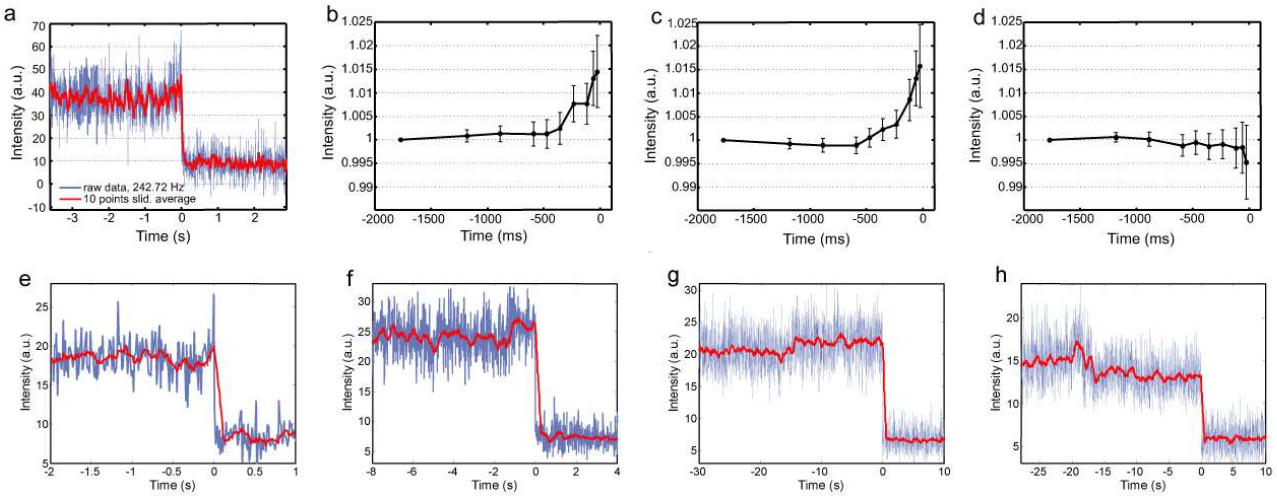

Fig. 4. Single DNA cleavage events monitored by plasmon coupling. (*a*) Cleavage trajectory recorded at 240 Hz using an intensified CCD detector. (*b*) Average scattering intensities at defined intervals preceding the dimer dissociation (0 ms) for 30 bps plasmon rulers (*c*) 40 bps plasmon rulers (*d*) 60 bps plasmon rulers (raw data recorded at 85 Hz). In (*b*) – (*d*) we set the time of the plasmon ruler dissociation equal to 0 ms and calculated the average intensities for shortening time intervals between [-1770 to 0] ms and [-24 to 0] ms. To account for different starting intensities we normalized the trajectories and set the average intensities of the longest time interval equal to one for each trajectory (total number of trajectories: 86 (30 bps), 96 (40 bps), 114 (60 bps). The error bars indicate the standard errors of the mean. Increasing scattering intensities for 30 and 40 bps spacers are consistent with a decreasing interparticle distance due to bending in the enzyme-DNA complex. For the 60 bps spacers the plasmon coupling is too weak to observe the bending (see text). The slight drop in the last data point of (*d*) is due to some uncertainty in defining the moment of dissociation. In some trajectories points during or shortly after the dissociation are picked leading to an overall lower scattering intensity. (*e*) – (*h*) Individual scattering trajectories for 40 bps plasmon rulers recorded at 85 Hz. The raw data are plotted in blue, sliding averages (over 10 frames (*e*), 25 frames (*f*), 50 frames (*g*)-(*h*) are included in red to guide the eye). A common feature observed in many trajectories is a slight increase in scattering intensity preceding the dimer dissociation (0s). The dwell times in the "high intensity" state range from a few ms (*e*) to hundreds of ms (*f*) to tens of seconds (*g*). (*h*) In about 4% of the recorded trajectories we first observe a slight drop in intensity previous to dimer dissociation. This is consistent with subsequent cleavage event in plasmon rulers with multiple tethers.

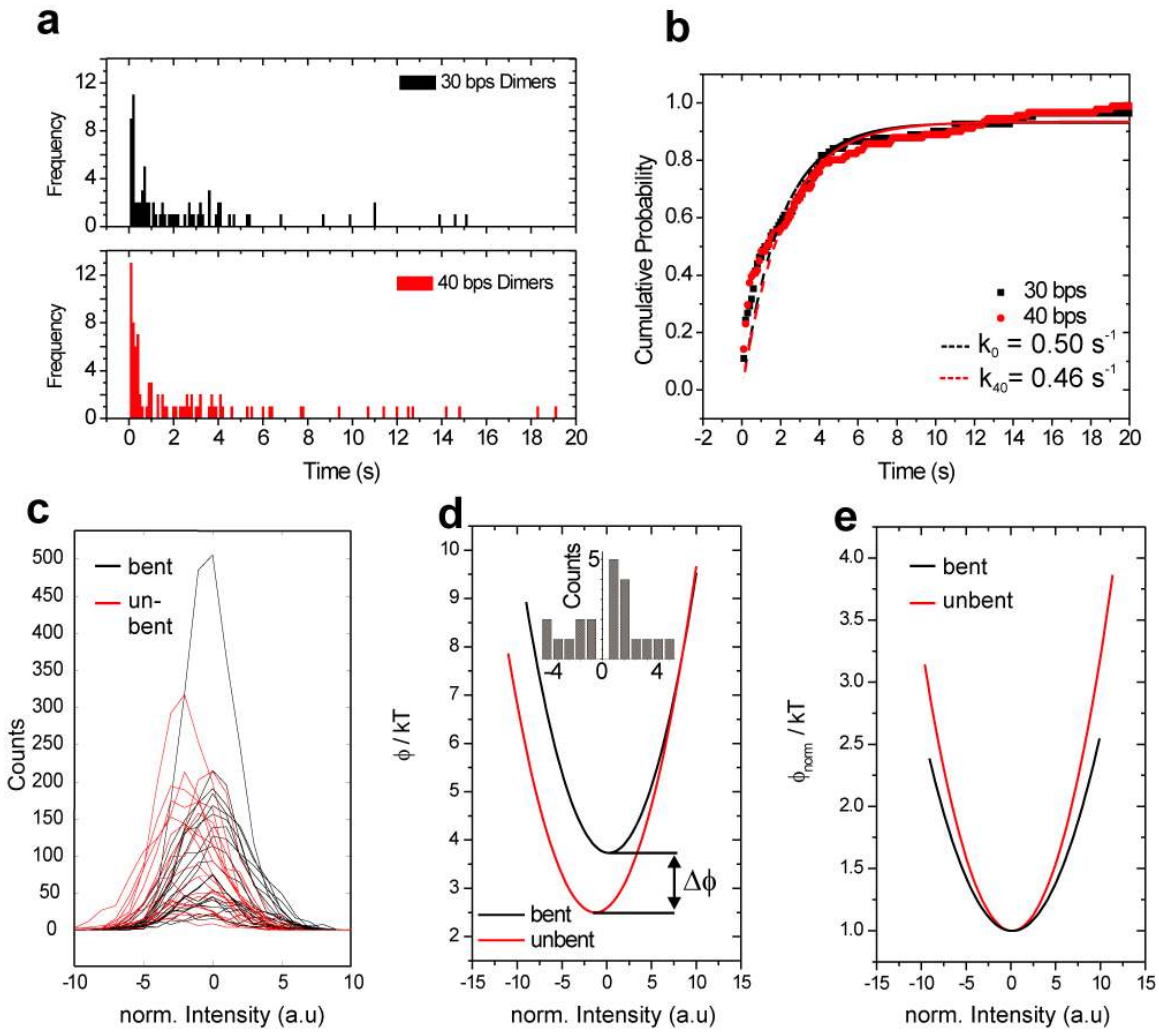

Fig. 5. Kinetic & thermodynamic analysis of single molecule data. (*a*)-(*b*) Dwell time analysis of plasmon rulers in high intensity state. (*a*) Histograms with a bin size of 100 ms for 30 bps plasmon rulers (top) and 40 bps plasmon rulers (bottom). (*b*) Cumulative probability of plasmon ruler dissociation. The plots show the percentage of dimers with dwell times less than the indicated time. First order kinetic fits have been included as dashed lines (k_{30} = 0.50 s^{-1}, k_{40} = 0.46 s^{-1}). (*c*) Histogram of normalized intensities for 21 individual cleavage trajectories of plasmon rulers with 40 bps DNA (selection criterion: system remains in bent state for more than 100 frames). The intensities are normalized to the maximum of the intensity distributions in the bent states (arbitrarily set to 0) The distributions of the bent state (black) are shifted to higher intensity values compared to the straight state (red). (*d*) Average interaction potentials of the particles in plasmon rulers with bent (black) and unbent (red) DNA spacer obtained from (*c*). The potential of the bent state is shifted to higher intensity (= shorter interparticle distance) and is offset in energy by $\Delta\phi = 1.2\ kT$. This energetic offset corresponds to the energy required for bending the DNA. The included histogram shows the intensity distribution of the penultimate frames before dimer dissociation for all 21 trajectories. (*e*) The superposition of the interparticle potentials of the bent and unbent states show that the width of the bent potential is larger, indicative of a decreased DNA spring constant in the bent state.

References

1. Itoh, H., Takahashi, A., Adachi, K., Noji, H., Yasuda, R., Yoshida, M. & Kinosita, K. (2004) *Nature* **427,** 465-468.
2. Kural, C., Kim, H., Syed, S., Goshima, G., Gelfand, V. I. & Selvin, P. R. (2005) *Science* **308,** 1469-1472.
3. Yildiz, A., Tomishige, M., Vale, R. D. & Selvin, P. R. (2004) *Science* **303,** 676-8.
4. Zhuang, X. W., Kim, H., Pereira, M. J. B., Babcock, H. P., Walter, N. G. & Chu, S. (2002) *Science* **296,** 1473-1476.
5. Bianco, P. R., Brewer, L. R., Corzett, M., Balhorn, R., Yeh, Y., Kowalczykowski, S. C. & Baskin, R. J. (2001) *Nature* **409,** 374-378.
6. Shivashankar, G. V. & Libchaber, A. (1998) *Biophysical Journal* **74,** A242-A242.
7. Giepmans, B. N. G., Adams, S. R., Ellisman, M. H. & Tsien, R. Y. (2006) *Science* **312,** 217-224.
8. Weiss, S. (2000) *Nature Structural Biology* **7,** 724-729.
9. Xie, X. S. & Lu, H. P. (1999) *Journal of Biological Chemistry* **274,** 15967-15970.
10. Weiss, S. (1999) *Science* **283,** 1676-1683.
11. Ha, T., Enderle, T., Ogletree, D. F., Chemla, D. S., Selvin, P. R. & Weiss, S. (1996) *PNAS* **93,** 6264-6268.
12. Dubois, A., Canva, M., Brun, A., Chaput, F. & Boilot, J. P. (1996) *Applied Optics* **35,** 3193-3199.
13. Sonnichsen, C., Reinhard, B. M., Liphardt, J. & Alivisatos, A. P. (2005) *Nature Biotechnology* **23,** 741-745.
14. Kelly, K. L., Coronado, E., Zhao, L. L. & Schatz, G. C. (2003) *Journal of Physical Chemistry B* **107,** 668-677.
15. Khlebtsov, B., Melnikov, A., Zharov, V. & Khlebtsov, N. (2006) *Nanotechnology* **17,** 1437-1445.
16. Elghanian, R., Storhoff, J. J., Mucic, R. C., Letsinger, R. L. & Mirkin, C. A. (1997) *Science* **277,** 1078-1081.
17. Nordlander, P. & Prodan, E. (2004) *Nano Letters* **4,** 2209-2213.
18. Maier, S. A., Brongersma, M. L., Kik, P. G. & Atwater, H. A. (2002) *Physical Review B* **65,** 193408.
19. Rechberger, W., Hohenau, A., Leitner, A., Krenn, J. R., Lamprecht, B. & Aussenegg, F. R. (2003) *Optics Communications* **220,** 137-141.
20. Prodan, E., Radloff, C., Halas, N. J. & Nordlander, P. (2003) *Science* **302,** 419-422.
21. Haynes, C. L., McFarland, A. D., Zhao, L. L., Van Duyne, R. P., Schatz, G. C., Gunnarsson, L., Prikulis, J., Kasemo, B. & Kall, M. (2003) *Journal of Physical Chemistry B* **107,** 7337-7342.
22. Reinhard, B. M., Siu, M., Agarwal, H., Alivisatos, A. P. & Liphardt, J. (2005) *Nano Letters* **5,** 2246-2252.
23. Kreibig, U. & Vollmer, M. (1995) *Optical Properties of Metal Clusters* (Springer, Berlin).
24. Halas, N. (2005) *Mrs Bulletin* **30,** 362-367.
25. Hirsch, L. R., Gobin, A. M., Lowery, A. R., Tam, F., Drezek, R. A., Halas, N. J. & West, J. L. (2006) *Ann Biomed Eng* **34,** 15-22.
26. Yguerabide, J. & Yguerabide, E. E. (1998) *Analytical Biochemistry* **262,** 157-176.
27. Bloomfield, V. A., Crothers, D. M. & Tinoco, J., Ignacio (2000) *Nucleic Acids, Structures, Properties, and Functions* (University Science Books, Sausalito).
28. Chen, L., Glover, J. N. M., Hogan, P. G., Rao, A. & Harrison, S. C. (1998) *Nature* **392,** 42-48.
29. Love, J. J., Li, X. A., Case, D. A., Giese, K., Grosschedl, R. & Wright, P. E. (1995) *Nature* **376,** 791-795.
30. Gartenberg, M. R. & Crothers, D. M. (1988) *Nature* **333,** 824-829.
31. Ansari, A. Z., Bradner, J. E. & Ohalloran, T. V. (1995) *Nature* **374,** 371-375.
32. Rappas, M., Schumacher, J., Beuron, F., Niwa, H., Bordes, P., Wigneshweraraj, S., Keetch, C. A., Robinson, C. V., Buck, M. & Zhang, X. D. (2005) *Science* **307,** 1972-1975.
33. Travers, A. & Drew, H. (1997) *Biopolymers* **44,** 423-433.
34. Smith, D. E., Tans, S. J., Smith, S. B., Grimes, S., Anderson, D. L. & Bustamante, C. (2001) *Nature* **413,** 748-752.
35. Perona, J. J. (2002) *Methods* **28,** 353-364.
36. Pingoud, A. & Jeltsch, A. (1997) *European Journal of Biochemistry* **246,** 1-22.

37. Wilcox, D. E. (1996) *Chemical Reviews* **96,** 2435-2458.
38. Vipond, I. B. & Halford, S. E. (1993) *Molecular Microbiology* **9,** 225-231.
39. Winkler, F. K., Banner, D. W., Oefner, C., Tsernoglou, D., Brown, R. S., Heathman, S. P., Bryan, R. K., Martin, P. D., Petratos, K. & Wilson, K. S. (1993) *Embo Journal* **12,** 1781-1795.
40. Perona, J. J. & Martin, A. M. (1997) *Journal of Molecular Biology* **273,** 207-225.
41. Zheng, M., Davidson, F. & Huang, X. Y. (2003) *Journal of the American Chemical Society* **125,** 7790-7791.
42. Johnson, P. B. & Christy, R. W. (1972) *Physical Review B* **6,** 4370-4379.
43. Vipond, I. B., Baldwin, G. S. & Halford, S. E. (1995) *Biochemistry* **34,** 697-704.
44. Kratky, O. & Porod, G. (1949) *Recueil Des Travaux Chimiques Des Pays-Bas-Journal of the Royal Netherlands Chemical Society* **68,** 1106-1122.
45. Smith, S. B., Cui, Y. J. & Bustamante, C. (1996) *Science* **271,** 795-799.
46. Hiller, D. A., Fogg, J. M., Martin, A. M., Beechem, J. M., Reich, N. O. & Perona, J. J. (2003) *Biochemistry* **42,** 14375-14385.
47. In the absence of divalent metal ions EcoRV endonuclease binds nonspecifically to DNA, with no preference for its recognition site over any other (Taylor et al. (1991) Biochemistry 30, 8743-8753). It is known from crystal structures that in non-cognate DNA-EcoRV restriction enzyme complexes the DNA retains a B configuration like structure and is not bent (Winkler et al (1993) EMBO Journal 12, 1781-1795.) This was confirmed by bulk FRET measurements that did not show an intensity change upon addition of EcoRV without divalent ions (Hiller et al (2003) Biochemistry 42, 14375-14385.
48. Waters, T. R. & Connolly, B. A. (1994) *Biochemistry* **33,** 1812-1819.
49. Baldwin, G. S., Vipond, I. B. & Halford, S. E. (1995) *Biochemistry* **34,** 705-714.
50. The gold probes might also slow the dynamics of the enzymatic reaction by perturbation of the two rate determining steps DNA hydrolysis and product release. Based on the Stokes-Einstein approximation, the diffusion coefficient of a free 40 nm particle in water at 298K is ~$1.1*10^{-11}$ m^2s and it has a root mean square displacement of 4.7 nm/μs. For the estimation of the force exerted on the DNA by the non-immobilized particles, we assume that the displacement occurs completely along the interparticle axis. In that case a pertubating force of about 1.6 pN could act on the enzyme-DNA complex. Wuite and coworkers investigated the efficiency of DNA cleavage by EcoRV under tension. Their studies show that the cleavage efficiency is not affected by forces significantly below 30 pN (van den Broek et al (2005), Nucleic Acids Research, 33, 2676-2684).
51. Singh-Zocchi, M., Dixit, S., Ivanov, V. & Zocchi, G. (2003) *PNAS* **100,** 7605-7610.
52. Zocchi, G. (2001) *Biophysical Journal* **81,** 2946-2953.
53. Bustamante, C., Bryant, Z. & Smith, S. B. (2003) *Nature* **421,** 423-427.
54. Li, Z., Jin, R. C., Mirkin, C. A. & Letsinger, R. L. (2002) *Nucleic Acids Research* **30,** 1558-1562.
55. Whitesides, G. M. & Laibinis, P. E. (1990) *Langmuir* **6,** 87-96.
56. Zanchet, D., Micheel, C. M., Parak, W. J., Gerion, D., Williams, S. C. & Alivisatos, A. P. (2002) *Journal of Physical Chemistry B* **106,** 11758-11763.
57. Sam, M. D. & Perona, J. J. (1999) *Biochemistry* **38,** 6576-6586.

Supporting Information for Reinhard *et al.*

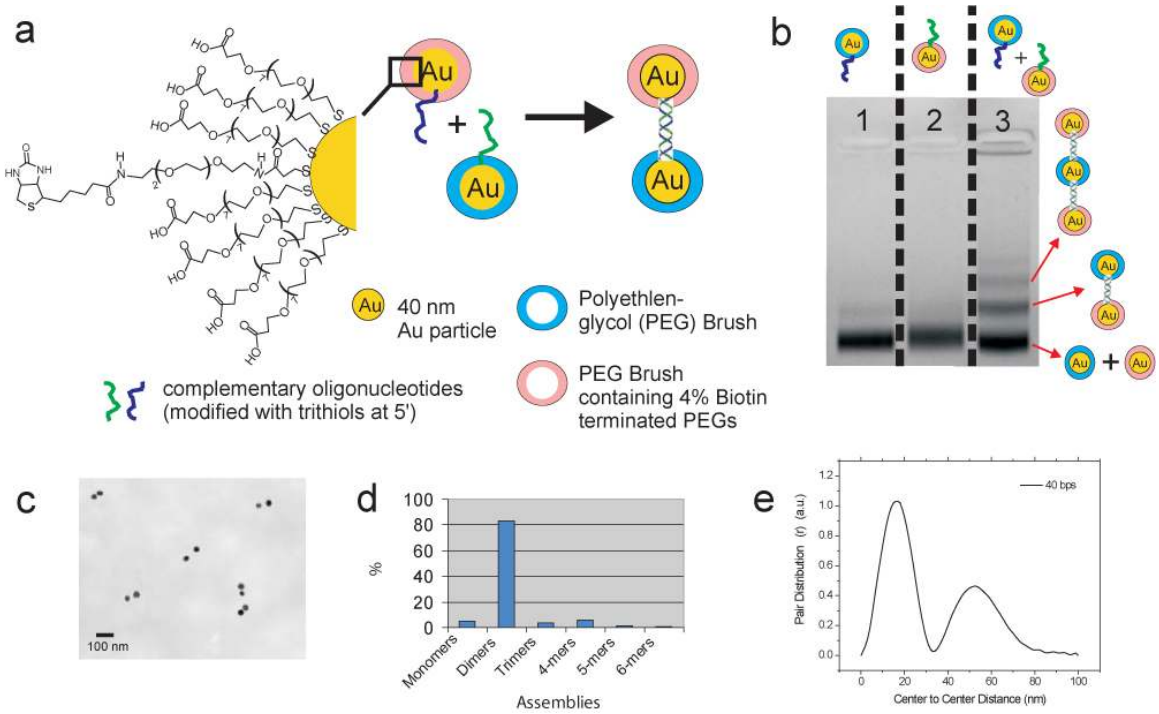

Fig. S1. Liquid Phase DNA-Programmed Assembly of Plasmon Rulers. (*a*) 40 nm gold particles passivated with PEG and functionalized with single stranded DNA (ssDNA) were obtained via subsequent ligand exchange reactions: Citrate ligands vs. BSPP, BSPP vs. DNA and finally BSPP vs. PEG. We synthesized two different flavors of particles per dimer: one with thiolated carboxy terminated PEGs (blue) and one with PEGs mixed 25:1 with a thiolated biotin terminated PEG (pink). These particles were stable in 500 mM NaCl for several days. In order to minimize multiple tether formation during hybridization of the gold-ssDNA conjugates, the ssDNA : particle ratio was limited to 25:1, which leads to a maximum surface coverage of 1 ssDNA / 201 nm^2. (*b*) After annealing overnight, dimers were separated from non-reacted monomers and larger assemblies by gel-electrophoresis and isolated by electroelution. (*c*) TEM micrograph of gel purified 60 bps dimers immobilized on a Neutravidin functionalized grid. The particles are arranged in pairs with distinct gaps between the individual particles. (*d*) TEM statistics of gel purified 60 bps dimers (total number of measured particles: 1055). The sample is highly enriched in dimers (82%), monomers and higher agglomerates are only minor impurities. (*e*) Pair distribution function of an aqueous solution (0.5x tris borate buffer) of 40 bps plasmon rulers obtained by small angle x-ray scattering (SAXS). The pair distribution function shows a center to center distance of ~52.4 nm. This confirms that the 40 nm particles are not touching but tethered by a double stranded DNA linker. Small Angle X-Ray data was collected using a Bruker Nanostar spectrometer fitted with a copper x-ray tube operating at 40kV and 35mA. The CuKα radiation (wavelength = 1.54 Å) was selected with graded multilayer cross-coupled Göbel mirrors. The scattered radiation was collected for five hours at a distance of 104.65 mm with a two-dimensional pressurized xenon gas detector (Bruker HiStar). The detector face had a diameter of 11.5 cm and a resolution of 1024 by 1024 pixels. A 2 mm beam stop (87% Pb, 13% Sb) is standard with the detector to prevent damage from the primary beam. Data were collected with a q range of approximately .01 $Å^{-1}$ to .21 $Å^{-1}$. The instrument is routinely calibrated using a silver behenate standard. The pair distribution function was calculated using the program GNOM (Svergun, D. I., *J. Appl. Cryst*. (1992), **25**, 495-503).

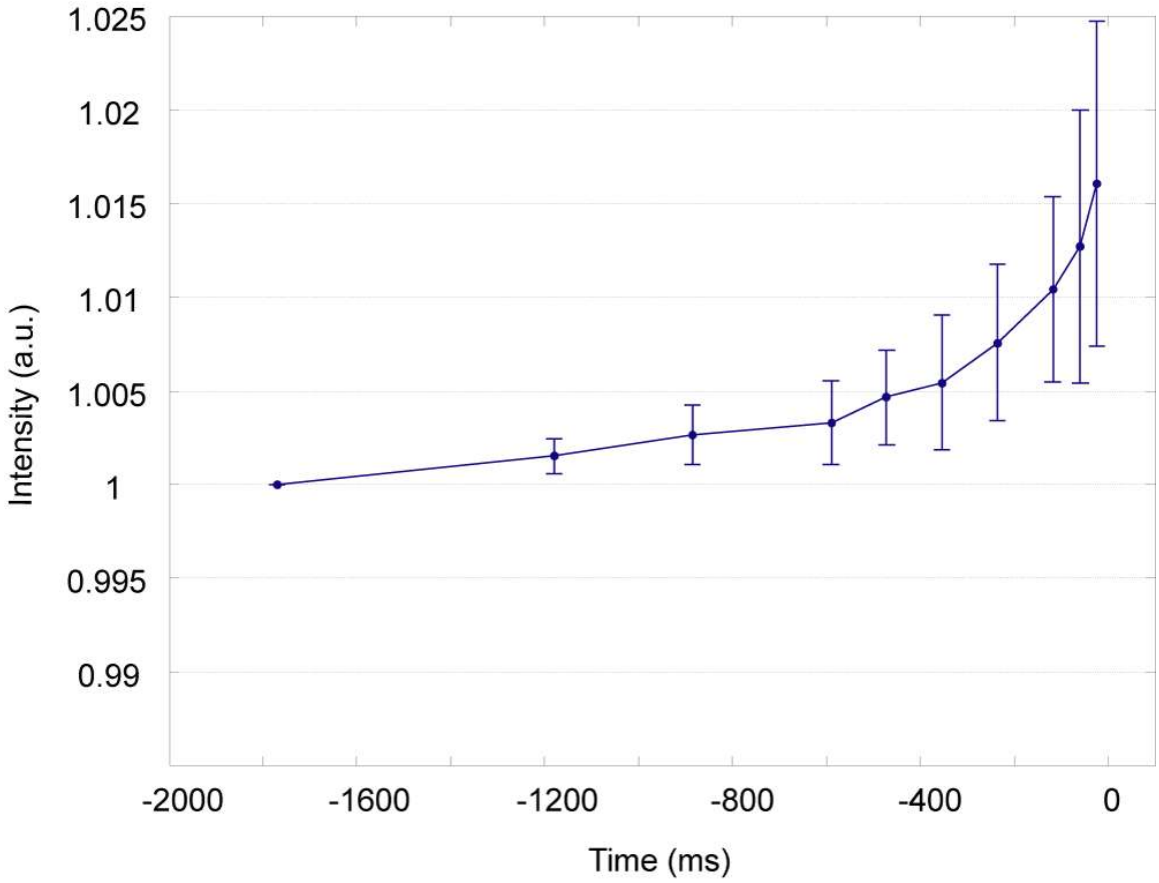

Fig. S2. Average scattering intensities at defined intervals preceding the dimer dissociation (0 ms) for 40 bps plasmon rulers under reaction conditions that decouple DNA binding and bending (bandwith: 85 Hz). The plasmon rulers are preincubated with EcoRV in Mg^{2+} free buffer, which allows the enzyme to bind but not to bend the DNA. Then the free enzyme is flushed out of the chamber and only after the unbound enzyme is removed, Mg^{2+} is added and the cleavage reaction is initiated. EcoRV is capable to bend DNA only in the presence of Mg^{2+}. Total number of trajectories: 68.

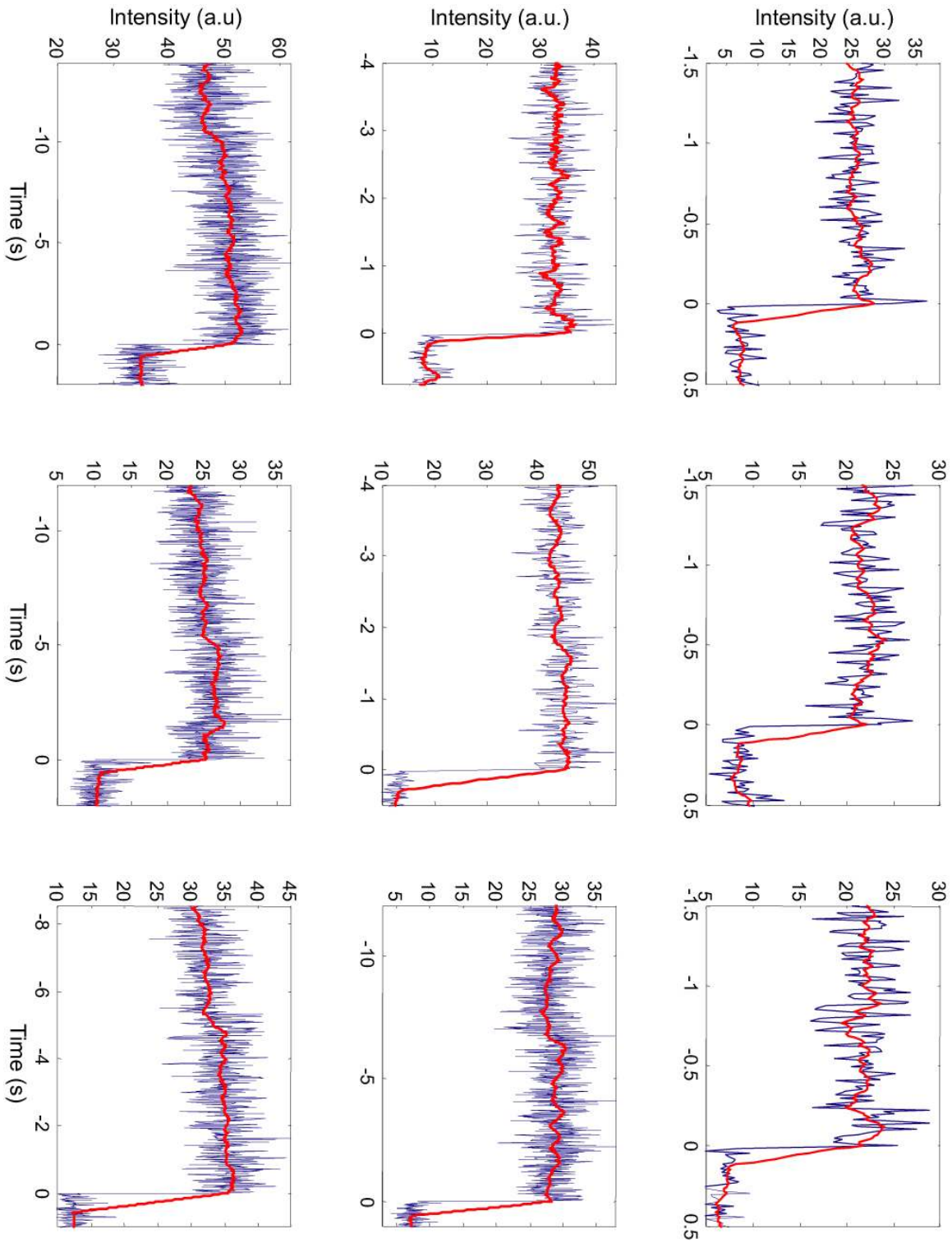

Fig. S3. Individual scattering trajectories for 40 bps plasmon rulers recorded at 85 Hz under reaction conditions that decouple DNA binding and bending (compare Fig. S2): the enzyme is bound to the plasmon rulers in the absence of Mg^{2+}. The trajectories show the same slight increase in scattering intensity preceding the dimer dissociation (0s) observed when EcoRV restriction was added in Mg^{2+} containing buffer (compare **Fig. 4**).